Nano-Micro Letters
e-ISSN 2150-5551
CN 31-2103/TB
ARTICLE
https://doi.org/10.1007/s40820-022-00929-y

Cite as
Nano-Micro Lett.
(2022) 14:195

Received: 24 May 2022
Accepted: 30 July 2022
Published online: 27 September 2022

Al_2O_3/HfO_2 Nanolaminate Dielectric Boosting IGZO-Based Flexible Thin-Film Transistors

Qiuwei Shi[1,2], Izzat Aziz[1], Jin-Hao Ciou[1], Jiangxin Wang[1], Dace Gao[1], Jiaqing Xiong[1], Pooi See Lee[1] ✉

HIGHLIGHTS

- A stable laminated Al_2O_3/HfO_2 insulator is developed by atomic layer deposition at a relatively lower temperature of 150 °C.
- The flexible thin-film transistors (TFTs) with bottom-gate top-contacted configuration are fabricated on a flexible substrate with the Al_2O_3/HfO_2 insulator.
- The flexible TFTs present the carrier mobilities of 9.7 $cm^2\ V^{-1}\ s^{-1}$, ON/OFF ratio of ~ 1.3×10^6, subthreshold voltage of 0.1 V, saturated current up to 0.83 mA, and subthreshold swing of 0.256 V dec^{-1}.

ABSTRACT Flexible thin-film transistors (TFTs) have attracted wide interest in the development of flexible and wearable displays or sensors. However, the conventional high processing temperatures hinder the preparation of stable and reliable dielectric materials on flexible substrates. Here, we develop a stable laminated Al_2O_3/HfO_2 insulator by atomic layer deposition at a relatively lower temperature of 150 °C. A sputtered amorphous indium-gallium-zinc oxide (IGZO) with the stoichiometry of $In_{0.37}Ga_{0.20}Zn_{0.18}O_{0.25}$ is used as the active channel material. The flexible TFTs with bottom-gate top-contacted configuration are further fabricated on a flexible polyimide substrate with the Al_2O_3/HfO_2 nanolaminates. Benefited from the unique structural and compositional configuration in the nanolaminates consisting of amorphous Al_2O_3, crystallized HfO_2, and the aluminate Al–Hf–O phase, the as-prepared TFTs present the carrier mobilities of 9.7 $cm^2\ V^{-1}\ s^{-1}$, ON/OFF ratio of ~ 1.3×10^6, subthreshold voltage of 0.1 V, saturated current up to 0.83 mA, and subthreshold swing of 0.256 V dec^{-1}, signifying a high-performance flexible TFT, which simultaneously able to withstand the bending radius of 40 mm. The TFTs with nanolaminate insulator possess satisfactory humidity stability and hysteresis behavior in a relative humidity of 60–70%, a temperature of 25–30 °C environment. The yield of IGZO-based TFTs with the nanolaminate insulator reaches 95%.

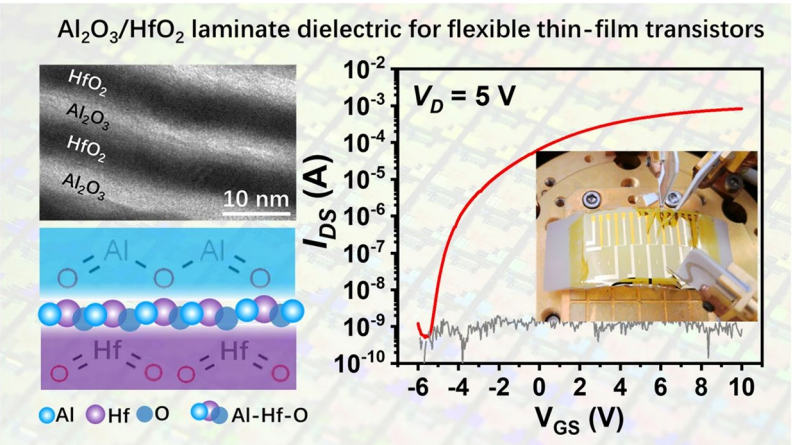

KEYWORDS Nanolaminate dielectric; Al_2O_3/HfO_2; Thin-film transistors; Flexible electronic

Qiuwei Shi and Izzat Aziz contributed equally to this work.
✉ Pooi See Lee, pslee@ntu.edu.sg
[1] School of Materials Science and Engineering, Nanyang Technological University, 50 Nanyang Avenue, Singapore 639798, Singapore
[2] School of Chemistry and Materials Science, Nanjing University of Information Science and Technology, Nanjing 210044, People's Republic of China

1 Introduction

The development and application of microelectronics have brought us to the era of digital and information age. Nowadays, thin-film transistors (TFTs) with the active channel layer of IGZO [1, 2], In_2O_3-ZnO, ZnO, and SnO_2 are the most basic and important component in modern electronic devices and equipments [3, 4], which have been widely used in sensors [5, 6], switching memories [7], logical circuits, and especially in flat-panel displays [8, 9]. The highly integrated portable electronic devices need high-performance TFTs, for example, in active matrix display for touch panels, flexible circuitries in smartphone, smartwatch, and laptop consumers products with features such as high brightness, high screen resolution and refresh rate, foldable, and low energy consumption. Thus, the great demand for flexible, high-performance, and high energy efficiency TFTs has emerged [10]. Recently, flexible electronics attracted great interest in the field of wearable health management devices and flexible displays for their intrinsic properties including bendable, deformable, and portable [11, 12]. Especially, as essential components of the pixel-drive circuits, TFTs work as the driving switches playing a significant role in organic light-emitting displays and liquid–crystal displays [9]. Accordingly, great efforts (such as the deep subthreshold regime operatable schottky-barrier IGZO thin-film transistor) are being conducted to develop low power, high current sensitivity, and flexible TFTs [13]. These high-performance flexible TFTs could be used as the key units for future displays, artificial skin, and soft robotics [14–17].

To date, combinations of advanced materials to fabricate flexible TFTs with enhanced intrinsic electrical properties and ingenious device structures with optimized configurations have been studied and explored. Despite many great progresses such as 1D carbon nanotubes (CNTs) or nanowire flexible TFTs [18–22], 2D nanomaterials flexible TFTs [23, 24], flexible organic TFTs [25–28], and metal-oxide flexible TFTs [29–31] have reported to obtain flexible TFTs. The developed flexible TFTs are still difficult to meet the practical application demands. This is due to the considerably the high standard and stringent requirements of electronic products ranging from superior electrical output performance, continuous/scale-up fabrication, reliability, and environmental stability. For CNTs flexible TFTs, although the single CNTs TFTs have been demonstrated with superior performance [32], but these is not suitable for assembling large-scale integrated circuits due to limiting factors such as cost, uniformity, and purity of network-type CNTs [19]. Regarding 2D materials TFTs, a wide variety of 2D nanosheets including boron nitride dielectric, graphene, MoS_2, and WS_2 channels can be used to prepare flexible TFTs with high mobilities [33], yet optimizing the flake sizes and continuous reliable operability are still needed to be explored. The organic semiconductors with intrinsic mechanical properties provide a promising way towards fabricating flexible TFTs. However, challenges such as environment robustness, shelf-life, and device performance are still needed to be circumvented. Comparing with the organic TFTs, metal-oxide flexible TFTs are compatible with conventional complementary metal–oxide–semiconductor processes and offer higher performance and stability [1, 34, 35], but typically need a relatively high-temperature annealing process [13, 36]. Usually, the polymeric substrates with relatively low glass transition temperature (T_g) such as polyethylene terephthalate (PET), polyethylene naphthalate (PEN), and polyimide (PI) for flexible TFTs are easily degraded during high-temperature processing [9, 31, 37]. Besides, the thermal explosion coefficient difference between layer for flexible TFTs will result in the internal stresses, decreasing the device performance and stability. Therefore, exploring flexible TFTs at low temperature (200 °C or lower) with ideal device performance is of considerable importance for flexible electronics.

In this work, high-performance flexible TFTs with bottom-gate top-contacted configuration were successfully fabricated on a polyimide substrate without any post-annealing process. The amorphous indium-gallium-zinc oxide (a-IGZO, with the stoichiometry of $In_{0.37}Ga_{0.20}Zn_{0.18}O_{0.25}$), was deposited by radio frequency (RF) sputtering and used as the active channel. The Al_2O_3/HfO_2 laminated insulator was prepared by atomic layer deposition (ALD) at a relatively lower temperature of 150 °C. Benefited from the nanolaminates of Al_2O_3/HfO_2 dielectric consisting of amorphous Al_2O_3 and crystallize HfO_2, and the interface aluminate Al–Hf–O phase, the as-prepared TFTs exhibited the carrier mobility of 9.7 $cm^2\ V^{-1}\ s^{-1}$, ON/OFF ratio ~ 1.3×10^6,

 https://doi.org/10.1007/s40820-022-00929-y

subthreshold voltage of 0.1 V, saturated current up to 0.70 mA, and subthreshold swing of 0.256 V dec^{-1}, as well as withstanding the bending radius of 40 mm. Furthermore, the TFTs with nanolaminate insulator possess satisfactory humidity stability and hysteresis behavior in a relative humidity of 60–70%, a temperature of 25–30 °C environment. The yield of IGZO-based TFTs with the nanolaminate insulator reaches 95%.

2 Experimental

2.1 Device Fabrication

Two types of substrates including the rigid Si wafers and flexible polyimide films were used for the TFTs fabrication. The detailed fabrication procedure for polyimide (PI) substrate-based flexible TFTs will be introduced below. First, the poly(pyromellitic dianhydride-co-4,4'-oxydianiline), amic acid (PAA) solution precursor (purchased from Sigma Aldrich) was spun coated onto the SiO_2/Si wafer at the spin rate of 1000 rpm for 1 min. Then, the PAA-coated wafer was moving into a tube furnace for annealing at 300 °C for 1 h with Ar flow for complete curing and imidization. The as-obtained PI film on the wafer was about 15 μm thick. Subsequently, the Ti/Au gate electrode with the thickness of 10/100 nm was deposited through an e-beam evaporator. A series of the thicker dielectric layers containing more layers of Al_2O_3/HfO_2 nanolaminate dielectric was used to fabricate the flexible TFTs. After a series of qualifications, the thickness of the nanolaminate dielectric was finally set at 20 nm. The nanolaminate Al_2O_3/HfO_2 (five layers composing of three layers of Al_2O_3 and two layers of HfO_2, the thickness of each layer is 4 nm) insulator was deposited using the Cambridge Nanotech ALD equipment using H_2O as the oxygen source, applying trimethylaluminum (TMA) and tetrakis(dimethylamido) hafnium (TDMAH) as their metal sources. Prior to deposition processing, the TDMAH was heated to 75 °C, while TMA and H_2O were kept at room temperature. The pulses sequence of one deposition cycle to obtain 0.1 nm Al_2O_3 was as follows: TMA exposure (0.25 s), N_2 purging (5 s), H_2O exposure (0.25 s), N_2 purging (5 s). The pulses sequence for obtaining 0.1 nm HfO_2 was as follows: TDMAH exposure (0.5 s), N_2 purging (5 s), H_2O exposure (0.1 s), N_2 purging (5 s). Afterward, a 50-nm-thick patterned IGZO channel layer was deposited at room temperature using the Denton Sputtering System. The process conditions applied for IGZO deposition include the pre-vacuum of 10^{-6} Torr, O_2 and Ar rate of 5 and 50 sccm, respectively, the RF sputtering power of 100 W. We have identified the structure and stoichiometry of the active layer (IGZO) with FIB-TEM and EDX. The red wireframe part in Fig. S1a shows that the IGZO active layer was in an amorphous state. The In/Ga/Zn/O atomic content percentage in IGZO was demonstrated as $In_{0.37}Ga_{0.20}Zn_{0.18}O_{0.25}$ (Fig. S1 and S2). Lastly, the patterned Ti/Au source and drain electrodes with the thickness of 10/100 nm were further deposited by E-beam evaporation, followed by lift-off to obtain the flexible TFTs for measurements. The channel length and width of TFT devices are 20 and 100 μm, respectively.

2.2 Film and Device Characterization

The microscope images were taken by the Olympus SZX16 optical microscope. All TFTs characterizations were performed using a Keithley 4200 semiconductor analyzer in ambient environment. The capacitances of the as-prepared insulators in metal–insulator–metal structures were measured by the Keysight (Agilent) LCR meter. The cross-sectional sample for transmission electron microscope (TEM) and energy-dispersive X-ray spectroscopy (EDS) measurements were prepared by a dual-beam FIB-SEM system (Zeiss Crossbeam 540). The TEM/EDS characterizations were carried out via the JEOL transmission electron microscope system at (JEM-2100 UHR at 200 kV and JED 2300 T EDS). X-ray photoelectron spectroscopy (XPS) of the as-prepared insulators was characterized with the PHI Quantera II surface analysis equipment. All the obtained XPS spectra were calibrated by the adsorbed C 1*s* (284.6 eV).

3 Results and Discussion

In this study, all the as-prepared TFTs with the bottom-gate top-contact configurations were fabricated by the typical photolithographic processes. The acceptable processing temperatures for obtaining an ideal insulator were discussed firstly. To study the area capacitance and leakage current density, the Al_2O_3 and HfO_2 insulators prepared at different temperatures were measured from the Au/insulator/Au structure (Fig. S3). As shown in Fig. S4–S6, the Al_2O_3 and HfO_2 insulators fabricated at a relatively lower temperature

at 150 °C exhibited promising insulating properties and capacitance. Inspired by the utilization of nanolaminate structure to achieve the highly dense, humidity/oxygen-resistant, and flexible thin films such as Al_2O_3/MgO [31], Al_2O_3/TiO_2 [38], and Al_2O_3/ZrO_2 [39], the laminated Al_2O_3/HfO_2 insulator with different layered numbers (Fig. S7) was fabricated here by controlling the ALD processing steps. The area capacitance and leakage current density of the different laminated Al_2O_3/HfO_2 insulators were further investigated (Fig. S8) The five layers laminated Al_2O_3/HfO_2 insulators showed the optimized insulating performance and reliability, which were labeled as Al_2O_3/HfO_2 nanolaminates and used for the TFTs preparation. As shown in Fig. 1a, the typical photolithographic processes were applied for preparing the PI-based flexible TFTs with the Al_2O_3/HfO_2 nanolaminates. The detailed procedures and parameters for each layer fabrication were depicted in the experimental section. The optical microscopic image of the as-prepared TFT device is given in Fig. 1b depicting the device with an effective channel length and width of 20 and 100 µm, respectively. After peeling off the PI substrate from the wafer, the as-fabricated PI-based flexible TFTs on a bending surface with a bending radius of 40 mm is displayed in Fig. 1c.

To demonstrate IGZO-based TFTs performances, comparisons were made with the 150 °C ALD-deposited insulators including Al_2O_3/HfO_2 nanolaminates, HfO_2, and Al_2O_3, and the electrical performance of the as-fabricated TFTs is measured and compared in Fig. 2, in which the I_{DS} (drain-to-source current), I_{GS} (gate leakage, drain-to-source current), and square-root-I_{DS} were plotted against the V_{GS} (gate-to-source voltage), and the I_{DS} was plotted against the V_{DS} (drain-to-source voltage). The thicknesses of the single layer HfO_2 and Al_2O_3 were 4 nm. Figure 2a, d, and g shows the transfer characteristics of the TFTs with Al_2O_3/HfO_2 nanolaminates, HfO_2, and Al_2O_3 insulators, respectively, in which the V_{DS} was fixed at 10 V. The leakage current was displayed in the range of about 10^{-9} A for these three samples. The maximum on-current (I_{on}) for the Al_2O_3/HfO_2 nanolaminates based TFTs was as high as 0.70 mA, which was 350% and 260% higher than those with Al_2O_3 (0.20 mA) HfO_2 (0.27 mA) insulators, respectively. As shown in Fig. 2b, e and h, the threshold voltage (V_{th}) of 0.1, 2.1, and 1.7 V for Al_2O_3/HfO_2 nanolaminates, HfO_2, and Al_2O_3-based TFTs was obtained from the intersection points of the linear fitted square-root-I_{DS} against V_{GS} respectively. Figure 2c, f and I shows the output characteristics of Al_2O_3/HfO_2 nanolaminates, HfO_2, and Al_2O_3-based TFTs with the applied V_{GS} from 2 to 10 V with the increasing steps of 2 V. The saturation current and pinch-off ranges of these three samples were clearly observed, indicating that the channel current could be well controlled by the V_{GS}. In addition,

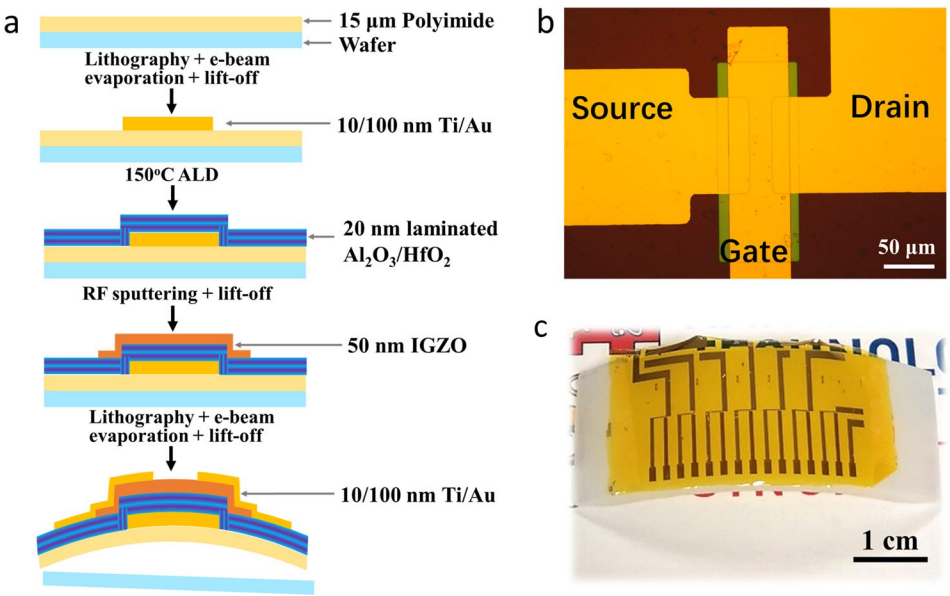

Fig. 1 **a** Schematic diagram of the fabrication flow of the IGZO-based TFT with laminated Al_2O_3/HfO_2 insulator including the respective thicknesses information. **b** The microscopic image of an as-prepared TFT device. **c** Photograph of the obtained TFTs with Al_2O_3/HfO_2 insulator on the flexible substrate

https://doi.org/10.1007/s40820-022-00929-y

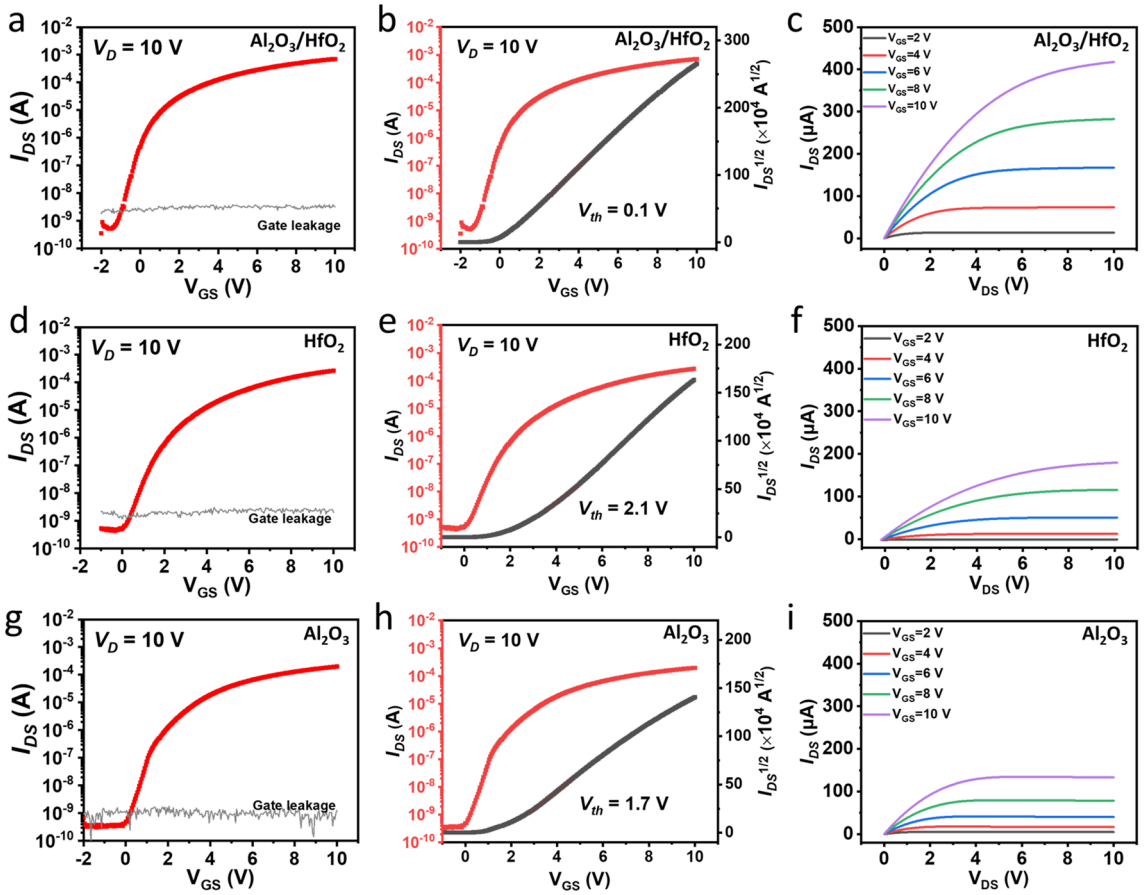

Fig. 2 Transfer characteristics, Sqrt (I_{DS}) curves, and output performances of the IGZO TFTs on the Si wafer with different insulators of **a–c** laminated Al_2O_3/HfO_2, **d–f** HfO_2, and **g–i** Al_2O_3 prepared by ALD at 150 °C

no current crowding behaviors for these three TFTs indicated good contact at the source/drain electrodes and channel interface. The I_{DS} of the TFTs with Al_2O_3/HfO_2 nanolaminates (0.42 mA) at the V_{GS} of 10 V was at least twice larger than that with HfO_2 (0.18 mA) and Al_2O_3 (0.13 mA) insulators, which could be attributed to the thermodynamical stability, high density, and good corrosion-resistance of Al_2O_3/HfO_2 nanolaminates and higher saturation carriers mobility [40]. The effective mobility (μ), subthreshold swing (*SS*), transconductance (g_m), and field-effect mobility (μ_{FE}) can be calculated by the following equations [40–42]:

$$I_D = \left(\frac{W}{2L}C_i\mu\right)\left(V_{GS} - V_{th}\right)^2 \quad (1)$$

$$SS = \frac{dV_{GS}}{d\left(\log I_D\right)} \quad (2)$$

$$g_m = \frac{W}{L}\mu C_i V_{DS} \quad (3)$$

$$\mu_{FE} = \frac{Lg_m}{WC_iV_{DS}\left(1 + \frac{V_E - V_{th}}{\mu}\frac{d\mu}{dV_{GS}}\right)} \quad (4)$$

where L and W are the length and width of the channel, C_i is the measured capacitance density (extracted from Fig. S2, S3, and S6 at the frequency of 100 kHz) of the insulator, I_D, V_{GS}, and V_{th} are the drain-to-source current, gate-to-source voltage, and threshold voltage, respectively. The calculated effective mobility μ for the TFTs with Al_2O_3/HfO_2 nanolaminates, HfO_2, and Al_2O_3 insulators was 9.7, 4.6, and 3.8 cm^2 V^{-1} s^{-1}, respectively. The calculated field-effect mobility for the TFTs with Al_2O_3/HfO_2 nanolaminates was 8.2 cm^2 V^{-1} s^{-1}. Figure S9 shows the V_{GS} against log-scale I_{DS} plots of the Al_2O_3/HfO_2 nanolaminates, HfO_2, and Al_2O_3 insulators based TFTs. The *SS* for the TFTs with the Al_2O_3/HfO_2 nanolaminates, HfO_2, and Al_2O_3 insulators was

256, 482, and 389 mV dec^{-1}. The performance parameters including μ, I_{ON}/I_{OFF} ratio, V_{th}, and SS at $V_{DS} = 10$ V of the TFTs are summarized in Table S1. In addition, the saturation currents per unit channel width of IGZO-based TFTs with different insulators are compared in Table 1. These results clearly indicated that the Al_2O_3/HfO_2 nanolaminates deposited using the low-temperature ALD have delivered a superior performance of the TFTs. Compared with other nanolaminates such as ZrO_2/Al_2O_3 (250 °C ALD) and Al_2O_3/MgO (70 °C ALD) [31, 43], the TFTs with Al_2O_3/HfO_2 nanolaminates exhibited promising saturation current which could be applied for driving the high-power electronic components.

To characterize the morphology and microstructure of the Al_2O_3/HfO_2 nanolaminates deposited via ALD at 150 °C, the cross-sectional TEM-EDS analysis was carried out on the IGZO/Al_2O_3/HfO_2 layers of an actual TFTs device. As shown in Fig. S10, the TEM specimen was firstly prepared by a dual-beam FIB system. The SEM image of the obtained FIB specimen was given in Fig. 3a. Figure 3b shows the cross-sectional TEM image of the Al_2O_3/HfO_2 nanolaminates. Five layers of the light (Al_2O_3) and dark (HfO_2) stacking structure with the total thickness of ~ 20 nm were well observed with minimal interfacial roughness and good thickness uniformity. As exhibited from the HRTEM image in Fig. 3c, the Al_2O_3 layers were found to be amorphous, whereas the lattice fringe of HfO_2 can be clearly observed indicating its crystalline state. In addition, a fuzzy interface between the crystallized HfO_2 and amorphous Al_2O_3 was formed, which might be attributed to the formation of the aluminate phase at the laminated interface (similar to Al–Mg-O aluminate phase) [31]. The FFT diffraction pattern in Fig. 3d evidently showed the single-crystalline nature of HfO_2 layers. The cross-sectional EDS mapping taken from part of the IGZO/Al_2O_3/HfO_2 actual TFTs displayed the distribution of Zn, In, Ga, Al, Hf, C, and O elements (Fig. 3e). Figure 3f–i exhibited the EDS maps of the Hf, Al, In, and O elements, respectively. The sublayer structure of the Al_2O_3/HfO_2 nanolaminates and sharper interface between the IGZO channel and insulator are found in Fig. 3f, h.

XPS spectra were also measured to investigate the elemental composition and chemical states of the Al_2O_3/HfO_2 nanolaminates, HfO_2, and Al_2O_3 insulators. As shown in Fig. 4a, the peaks corresponding to C, O, Al, and Hf elements were found in the Al_2O_3/HfO_2 nanolaminates XPS spectrum. The peaks belonging to C, O, and Hf elements and peaks corresponding to C, O, and Al elements were observed in the HfO_2 and Al_2O_3 XPS spectra, respectively. The O 1 *s* XPS spectra of the Al_2O_3/HfO_2 nanolaminates and Al_2O_3 are shown in Fig. 4b and fitted by two peak components through Gaussian fitting. The peaks centered at high binding energy of 532.1 eV correspond to oxygen vacancy, whereas the

Table 1 Comparison of the saturation current per unit channel width of IGZO-based TFTs with different insulators

Channel length/width (μm)	Insulators materials	V_{GS} (V)	V_{DS} (V)	Saturated current per unit width (μA $μm^{-1}$)	Refs.
60/1500	$HfO_xN_y/HfO_2/HfO_xN_y$	5	5	0.2	[46]
300/1000	Nd: Al_2O_3	10	10.1	0.06	[47]
30/100	Al_2O_3	1	0.5	0.04	[48]
100/1000	ZrO_2/HfO_2	20	20	1.2	[40]
10/20	AlO_x:Nd	10	5	0.5	[9]
50/500	Al_2O_3/MgO	10	10.1	1	[31]
10/50	SiO_x	30	10.1	0.4	[36]
100/1500	Al_2O_3/TiO_2	20	20	0.015	[38]
100/1000	SiO_2	20	5	0.1	[44]
7/50	$YAlO_x$	3	0.5	0.3	[30]
200/1000	$HfGdO_x$	4	10	0.1	[50]
50/500	Annealed Al_2O_3	3	2	0.7	[51]
100/1000	Y_2O_3	30	20	0.1	[52]
300/1000	SiO_2	30	5	0.3	[53]
250/1000	SiO_2	40	40	0.25	[54]
100/150	HfO_2	8	14	5.9	[55]
20/100	Al_2O_3/HfO_2 nanolaminates	10	10	7.03	This work

https://doi.org/10.1007/s40820-022-00929-y

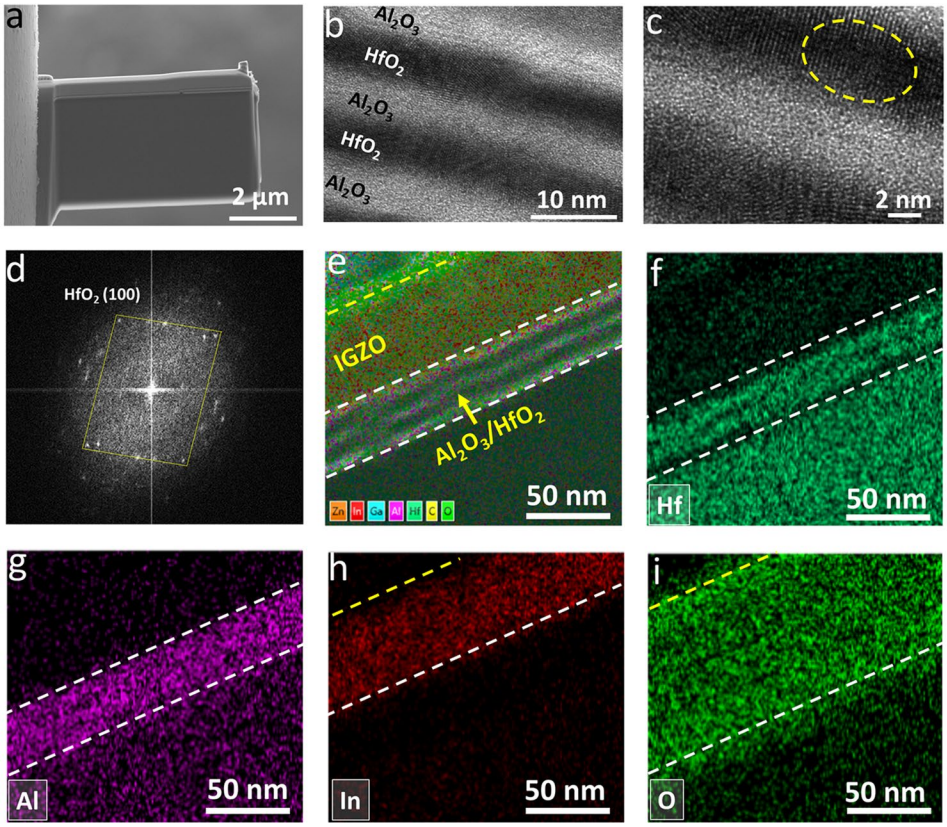

Fig. 3 **a** SEM image of the TEM specimen prepared by FIB. **b** Cross-sectional TEM and **c** HRTEM images of the laminated Al_2O_3/HfO_2 insulator prepared via ALD at 150 °C. **d** The fast fourier transform (FFT) diffraction pattern image obtained from the dotted area in panel **c**. **e** Cross-sectional TEM-EDS elemental mapping of elements Zn, In, Ga, Al, Hf, C, and O. EDS mapping of elements **f** Hf, **g** Al, **h** In, and **i** O

peaks at 530.9 eV are related to oxide lattices (metal-oxide bonds here) [40]. The relative content of oxygen vacancy for Al_2O_3/HfO_2 nanolaminates was found to be 23.2%, which was smaller than that of 40.6% for Al_2O_3. The Al_2O_3/HfO_2 nanolaminates with low oxygen vacancy were beneficial for enhancing the TFTs performance [40, 44]. Figure 4c, d presents the Al 2*p* and Hf 4*f* core-level XPS spectra for the Al_2O_3/HfO_2 nanolaminates, Al_2O_3, and HfO_2. The core-level peaks of Al 2*p* and Hf 4*f* in Al_2O_3 and HfO_2 were found at 74.5 eV (Al 2*p*), 18.4 eV (Hf $4f_{5/2}$), and 16.7 eV (Hf $4f_{7/2}$), in agreement with the binding energy in previous reports [45]. As for the Al_2O_3/HfO_2 nanolaminates comparing with Al_2O_3 and HfO_2, the Al 2*p* core-level peak was shifted toward lower binding energy of 74.5 eV, and Hf 4*f* core-level peaks were shifted toward higher binding energy of 18.8 eV (Hf 4f 5/2) and 17.1 eV (Hf $4f_{7/2}$). These binding energy shifts of Al 2*p* and Hf 4*f* in Al_2O_3/HfO_2 nanolaminates are resulted from the difference in electronegativities of Al (1.61) and Hf (1.32) [31, 46]. Therefore, as schematically shown in Fig. 4e, the aluminate phase of Al–Hf–O was formed between the sublayers of Al_2O_3 and HfO_2 in Al_2O_3/HfO_2 nanolaminates. These aluminate phases with enhanced thermodynamical stability, high density, and good corrosion-resistance have been reported in similar laminated structures such as Al_2O_3/ZrO_2, Al_2O_3/TiO_2, and Al_2O_3/MgO [31, 38, 39]. As a result, this Al–Hf–O chemical bonding improved the reliability of the laminated Al_2O_3/HfO_2 insulator. Therefore, the Al_2O_3/HfO_2 nanolaminates with the layered structure of amorphous Al_2O_3, the aluminate phase in sublayers, and crystallized HfO_2 could be applied as an ideal dielectric for the high-performance TFTs.

The flexible TFTs on the PI substrate were fabricated with 150 °C ALD-deposited Al_2O_3/HfO_2 nanolaminates. As shown in Fig. 5a, the PI-based flexible TFTs with Al_2O_3/HfO_2 nanolaminates could be tested on a bending surface with a bending radius of 40 mm. Figure 5b presents the transfer characteristics of the PI-based flexible TFTs with the fixed V_{DS} of 3 V. The leakage current was in the range

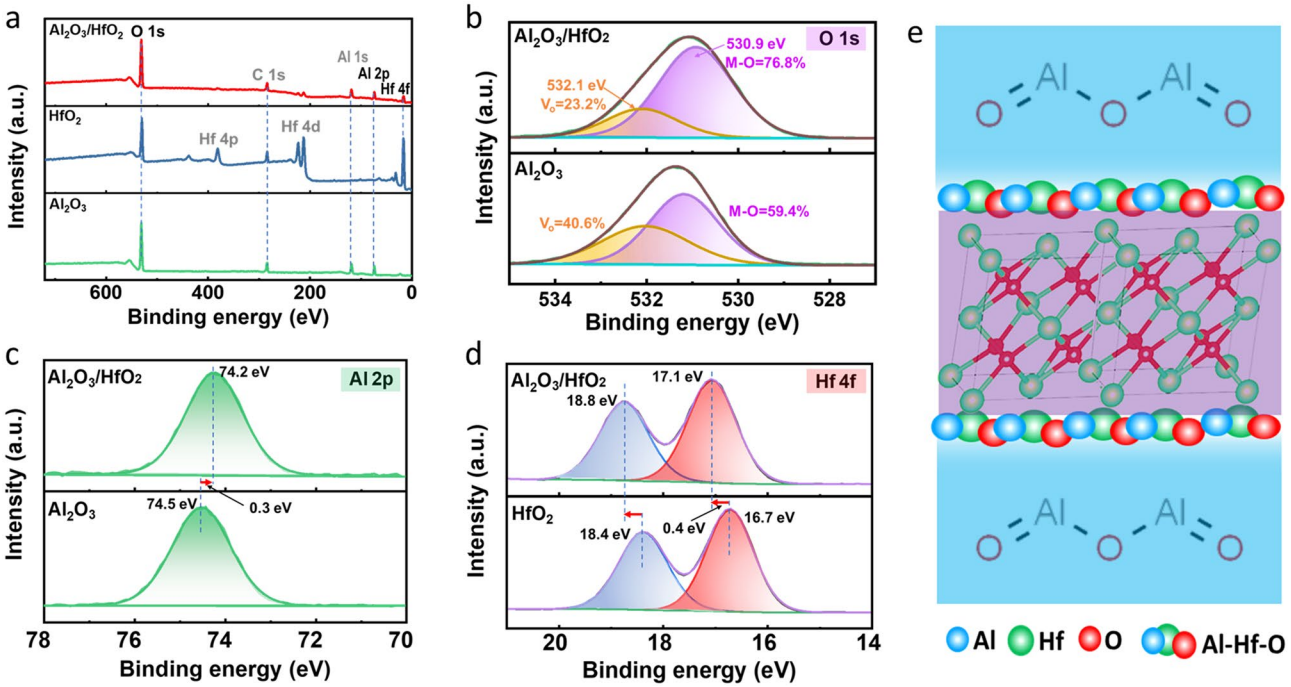

Fig. 4 **a** X-ray photoelectron spectra of the Al_2O_3/HfO_2, HfO_2, and Al_2O_3 insulators prepared by ALD at 150 °C. High-resolution **b** O 1*s* and **c** Al 2*p* spectra of the Al_2O_3/HfO_2 nanolaminates and Al_2O_3. **d** High-resolution Hf 4*f* spectra of the Al_2O_3/HfO_2 nanolaminates and HfO_2. **e** Schematic of the Al_2O_3/HfO_2 nanolaminates with amorphous Al_2O_3, crystallized HfO_2, and the aluminate (Al–Mg–O) phase at the interface

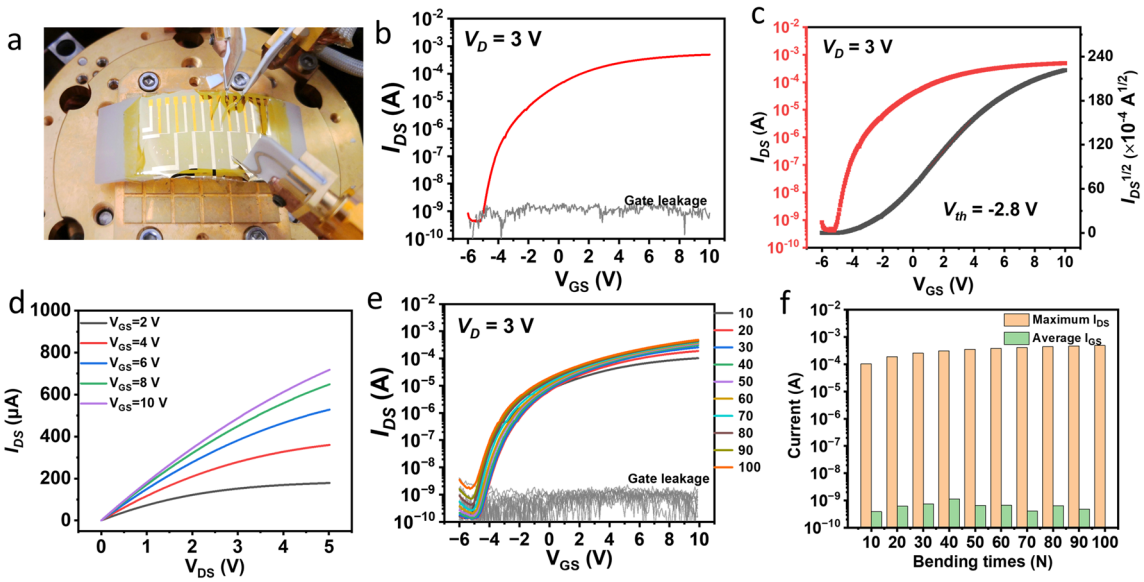

Fig. 5 **a, g** Photograph of the PI-based flexible TFTs with lAl_2O_3/HfO_2 nanolaminates tested on a bending surface with a bending radius of 40 mm. **b** Transfer characteristics, **c** Sqrt (I_{DS}) curve, and **d** output performances of the flexible TFTs tested at a bending radius of 40 mm. **e** Transfer characteristics and **f** the maximum IDS and average IGS of the flexible IGZO-based TFTs after repeated bending for 100 times at the bending radius of 40 mm

 https://doi.org/10.1007/s40820-022-00929-y

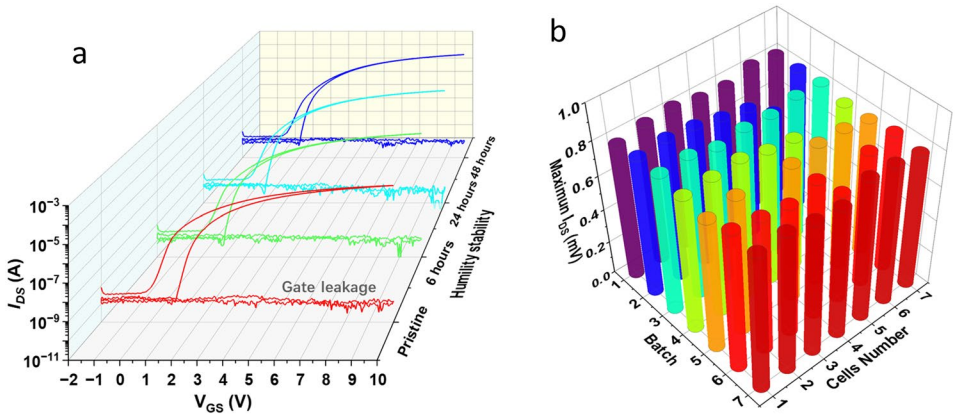

Fig. 6 **a** Transfer characteristics and hysteresis behavior of the IGZO-based TFTs with nanolaminate Al_2O_3/HfO_2 insulator in a pristine state and after being stored in a laboratory environment (relative humidity of 60–70%, temperature of 25–30 °C) for 6, 24, and 48 h. **b** 3D bars map showing maximum I_{DS} for 7 batch (each batch has seven cells) IGZO-based TFTs

of ~ 10^{-9} A. The maximum I_{on} for PI-based flexible TFTs was up to as 0.83 mA. The obtained I_{ON}/I_{OFF} ratio was higher than 10^6. The V_{th} of − 2.8 V was extracted from the intersection point of the linear fitted square-root-I_{DS} against V_{GS} (Fig. 5c). Figure 5d shows the output characteristics of Al_2O_3/HfO_2 nanolaminates-based flexible TFTs with the applied V_{GS} from 2 to 10 V with the increasing steps of 2 V. The saturation I_{DS} could be observed from the output curves. The I_{DS} of this flexible TFTs was up to 0.72 mA at the V_{GS} of 10 V. In addition, the V_{GS} against log-scale I_{DS} curves of the flexible TFTs are also plotted in Fig. S11. Based on Eq. (2), the *SS* of this flexible TFTs with the Al_2O_3/HfO_2 nanolaminates was calculated as 319 mV dec^{-1}. Compared with other PI-based organic or inorganic flexible TFTs [30, 37], the flexible TFTs with Al_2O_3/HfO_2 nanolaminates showed promising performance including the carriers mobility and output current. Transfer characteristics of the fabricated flexible IGZO thin-film transistors after repeated bending for 100 times at the bending radius of 40 mm are shown in Fig. 5e. Furthermore, the stable maximum I_{DS} and average gate leakage of the as-prepared TFTs are also summarized in Fig. 5f. These satisfactory electrical performances of the flexible IGZO-based TFTs exhibited their promising flexibility and endurability.

The humidity stability and hysteresis behavior of the as-prepared IGZO-based TFTs with nanolaminate Al_2O_3/HfO_2 insulator were conducted by storing the devices in a laboratory environment (relative humidity of 60–70%, temperature of 25–30 °C) at different times. As shown in Fig. 6a, the gate leakage of IGZO-based TFTs with nanolaminate Al_2O_3/HfO_2 insulator is kept stable and at a relatively low value of about 10^{-10} A. Meanwhile, the TFTs exhibited ideal transfer behaviors with small hysteresis after exposure to a relative humidity of 60–70%, and a temperature of 25–30 °C environment for 48 h. The reliability of the set of IGZO-based TFTs with nanolaminate Al_2O_3/HfO_2 insulator was also processed (Fig. 6b). Seven batches (each batch has seven cells) total of 49 IGZO-based TFT cells were tested. As shown in Fig. 6b, two cells in batch 3 and batch 4 were damaged. The other 47 cells worked well with an average maximum I_{DS} of 0.79 mV. The yield of IGZO-based TFTs with nanolaminate Al_2O_3/HfO_2 insulator reaches 95%.

4 Conclusions

Flexible TFTs on PI substrates were successfully fabricated using the Al_2O_3/HfO_2 nanolaminate which was deposited by ALD at 150 °C. The Al_2O_3/HfO_2 nanolaminate was demonstrated with the layered structure of amorphous Al_2O_3, crystallized HfO_2, and the aluminate Al–Hf–O phase at sublayers interface. The as-prepared TFTs without any post-annealing presented the carrier mobility of 9.7 cm^2 V^{-1} s^{-1}, ON/OFF ratio ~ 1.3×10^6, subthreshold voltage of 0.1 V, saturated current up to 0.83 mA, and subthreshold swing of 0.256 V dec^{-1}, as well as withstand the bending radius of 40 mm. The as-prepared TFTs possess satisfactory humidity stability in a relative humidity of 60–70%, a temperature of 25–30 °C environment. The yield of IGZO-based TFTs with the nanolaminate insulator

reaches 95%. We believe this Al_2O_3/HfO_2 nanolaminate could be one of the ideal candidates for high-performance electronics.

Acknowledgements This work was supported by the Competitive Research Program (Award No. NRF-CRP13-2014-02), RIE2020 ASTAR AME IAF-ICP (I1801E0030), and Campus for Research Excellence and Technological Enterprise (CREATE) that was supported by the National Research Foundation, Prime Minister's Office, Singapore. Q.W.S. thanks to the Natural Science Foundation of China (52003122) and the "Longshan scholar" start-up foundation of NUIST.

Funding Open access funding provided by Shanghai Jiao Tong University.

Supplementary Information The online version contains supplementary material available at https://doi.org/10.1007/s40820-022-00929-y.

References

1. M. Moreira, E. Carlos, C. Dias, J. Deuermeier, M. Pereira et al., Tailoring IGZO composition for enhanced fully solution-based thin film transistors. Nanomaterials **9**(9), 1273 (2019). https://doi.org/10.3390/nano9091273
2. A. Olziersky, P. Barquinha, A. Vilà, C. Magaña, E. Fortunato et al., Role of Ga_2O_3–In_2O_3–ZnO channel composition on the electrical performance of thin-film transistors. Mater. Chem. Phys. **131**, 512–518 (2011). https://doi.org/10.1016/j.matchemphys.2011.10.013
3. K. Myny, The development of flexible integrated circuits based on thin-film transistors. Nat. Electron. **1**, 30–39 (2018). https://doi.org/10.1038/s41928-017-0008-6
4. P. Yang, J. Zha, G. Gao, L. Zheng, H. Huang et al., Growth of tellurium nanobelts on h-BN for P-type transistors with ultrahigh hole mobility. Nano-Micro Lett. **14**, 109 (2022). https://doi.org/10.1007/s40820-022-00852-2
5. S. Wang, J. Xu, W. Wang, G.N. Wang, R. Rastak et al., Skin electronics from scalable fabrication of an intrinsically stretchable transistor array. Nature **555**, 83–88 (2018). https://doi.org/10.1038/nature25494
6. S. Jeon, S.E. Ahn, I. Song, C.J. Kim, U.I. Chung et al., Gated three-terminal device architecture to eliminate persistent photoconductivity in oxide semiconductor photosensor arrays. Nat. Mater. **11**, 301–305 (2012). https://doi.org/10.1038/nmat3256
7. L. Wang, W. Liao, S.L. Wong, Z.G. Yu, S. Li et al., Artificial synapses based on multiterminal memtransistors for neuromorphic application. Adv. Funct. Mater. **29**(25), 1901106 (2019). https://doi.org/10.1002/adfm.201901106
8. N. Cui, H. Ren, Q. Tang, X. Zhao, Y. Tong et al., Fully transparent conformal organic thin-film transistor array and its application as LED front driving. Nanoscale **10**, 3613–3620 (2018). https://doi.org/10.1039/c7nr09134f
9. H. Xu, D. Luo, M. Li, M. Xu, J. Zou et al., A flexible AMOLED display on the PEN substrate driven by oxide thin-film transistors using anodized aluminium oxide as dielectric. J. Mater. Chem. C **2**, 1255–1259 (2014). https://doi.org/10.1039/c3tc31710b
10. P. Barquinha, L. Pereira, G. Gonçalves, R. Martins, D. Kuščer et al., Performance and stability of low temperature transparent thin-film transistors using amorphous multicomponent dielectrics. J. Electrochem. Soc. **156**, H824 (2009). https://doi.org/10.1149/1.3216049
11. L. Li, Y. Liu, C. Song, S. Sheng, L. Yang et al., Wearable alignment-free microfiber-based sensor chip for precise vital signs monitoring and cardiovascular assessment. Adv. Fiber Mater. **4**, 475–486 (2022). https://doi.org/10.1007/s42765-021-00121-8
12. Z. Zhang, Y. Kang, N. Yao, J. Pan, W. Yu et al., A multifunctional airflow sensor enabled by optical micro/nanofiber. Adv. Fiber Mater. **3**, 359–367 (2021). https://doi.org/10.1007/s42765-021-00097-5
13. S. Lee, A. Nathan, Subthreshold Schottky-barrier thin-film transistors with ultralow power and high intrinsic gain. Science **354**(6310), 302–304 (2016). https://doi.org/10.1126/science.aah5035
14. Z.W.K. Low, Z. Li, C. Owh, P.L. Chee, E. Ye et al., Using artificial skin devices as skin replacements: insights into superficial treatment. Small **15**(9), 1805453 (2019). https://doi.org/10.1002/smll.201805453
15. H. Shim, K. Sim, F. Ershad, P. Yang, A. Thukral et al., Stretchable elastic synaptic transistors for neurologically integrated soft engineering systems. Sci. Adv. **5**, eaax4961 (2019). https://doi.org/10.1126/sciadv.aax4961
16. I. Cunha, R. Barras, P. Grey, D. Gaspar, E. Fortunato et al., Reusable cellulose-based hydrogel sticker film applied as gate dielectric in paper electrolyte-gated transistors. Adv. Funct. Mater. **27**(16), 1606755 (2017). https://doi.org/10.1002/adfm.201606755
17. E. Carlos, R. Branquinho, R. Martins, E. Fortunato, New challenges of printed high-κ oxide dielectrics. Solid State

Electron. **183**, 108044 (2021). https://doi.org/10.1016/j.sse.2021.108044

18. T. Lei, L.L. Shao, Y.Q. Zheng, G. Pitner, G. Fang et al., Low-voltage high-performance flexible digital and analog circuits based on ultrahigh-purity semiconducting carbon nanotubes. Nat. Commun. **10**, 2161 (2019). https://doi.org/10.1038/s41467-019-10145-9
19. L.M. Peng, Z. Zhang, C. Qiu, Carbon nanotube digital electronics. Nat. Electron. **2**, 499–505 (2019). https://doi.org/10.1038/s41928-019-0330-2
20. F. Xu, M.Y. Wu, N.S. Safron, S.S. Roy, R.M. Jacobberger et al., Highly stretchable carbon nanotube transistors with ion gel gate dielectrics. Nano Lett. **14**, 682–686 (2014). https://doi.org/10.1021/nl403941a
21. D.M. Sun, C. Liu, W.C. Ren, H.M. Cheng, A review of carbon nanotube- and graphene-based flexible thin-film transistors. Small **9**(8), 1188–1205 (2013). https://doi.org/10.1002/smll.201203154
22. S. Ju, A. Facchetti, Y. Xuan, J. Liu, F. Ishikawa et al., Fabrication of fully transparent nanowire transistors for transparent and flexible electronics. Nat. Nanotechnol. **2**, 378–384 (2007). https://doi.org/10.1038/nnano.2007.151
23. R. Cheng, S. Jiang, Y. Chen, Y. Liu, N. Weiss et al., Few-layer molybdenum disulfide transistors and circuits for high-speed flexible electronics. Nat. Commun. **5**, 5143 (2014). https://doi.org/10.1038/ncomms6143
24. S.K. Lee, H.Y. Jang, S. Jang, E. Choi, B.H. Hong et al., All graphene-based thin film transistors on flexible plastic substrates. Nano Lett. **12**, 3472–3476 (2012). https://doi.org/10.1021/nl300948c
25. H. Matsui, Y. Takeda, S. Tokito, Flexible and printed organic transistors: from materials to integrated circuits. Org. Electron. **75**, 105432 (2019). https://doi.org/10.1016/j.orgel.2019.105432
26. J. Kwon, Y. Takeda, R. Shiwaku, S. Tokito, K. Cho et al., Three-dimensional monolithic integration in flexible printed organic transistors. Nat. Commun. **10**, 54 (2019). https://doi.org/10.1038/s41467-018-07904-5
27. H. Ren, N. Cui, Q. Tang, Y. Tong, X. Zhao et al., High-performance, ultrathin, ultraflexible organic thin-film transistor array via solution process. Small **14**(33), 1801020 (2018). https://doi.org/10.1002/smll.201801020
28. H. Chen, W. Zhang, M. Li, G. He, X. Guo, Interface engineering in organic field-effect transistors: principles, applications, and perspectives. Chem. Rev. **120**, 2879–2949 (2020). https://doi.org/10.1021/acs.chemrev.9b00532
29. X. Chen, G. Zhang, J. Wan, T. Guo, L. Li et al., Transparent and flexible thin-film transistors with high performance prepared at ultralow temperatures by atomic layer deposition. Adv. Electron. Mater. **5**(2), 1800583 (2019). https://doi.org/10.1002/aelm.201800583
30. S. Bolat, P. Fuchs, S. Knobelspies, O. Temel, G.T. Sevilla et al., Inkjet-printed and deep-UV-annealed $YAlO_x$ dielectrics for high-performance IGZO thin-film transistors on flexible substrates. Adv. Electron. Mater. **5**(6), 1800843 (2019). https://doi.org/10.1002/aelm.201800843
31. J.H. Kwon, J. Park, M.K. Lee, J.W. Park, Y. Jeon et al., Low-temperature fabrication of robust, transparent, and flexible thin-film transistors with a nanolaminated insulator. ACS Appl. Mater. Interfaces **10**(18), 15829–15840 (2018). https://doi.org/10.1021/acsami.8b01438
32. C. Qiu, Z. Zhang, M. Xiao, Y. Yang, D. Zhong et al., Scaling carbon nanotube complementary transistors to 5-nm gate lengths. Science **355**(6322), 271–276 (2017). https://doi.org/10.1126/science.aaj1628
33. D. Akinwande, N. Petrone, J. Hone, Two-dimensional flexible nanoelectronics. Nat. Commun. **5**, 5678 (2014). https://doi.org/10.1038/ncomms6678
34. E. Fortunato, P. Barquinha, R. Martins, Oxide semiconductor thin-film transistors: a review of recent advances. Adv. Mater. **24**(22), 2945–2986 (2012). https://doi.org/10.1002/adma.201103228
35. P. Barquinha, L. Pereira, G. Gonçalves, R. Martins, E. Fortunato, Toward high-performance amorphous GIZO TFTs. J. Electrochem. Soc. **156**, H161 (2009). https://doi.org/10.1149/1.3049819
36. M. Kim, J.H. Jeong, H.J. Lee, T.K. Ahn, H.S. Shin et al., High mobility bottom gate InGaZnO thin film transistors with SiO_x etch stopper. Appl. Phys. Lett. **90**, 212114 (2007). https://doi.org/10.1063/1.2742790
37. A. Gumyusenge, X. Luo, Z. Ke, D.T. Tran, J. Mei, Polyimide-based high-temperature plastic electronics. ACS Mater. Lett. **1**, 154–157 (2019). https://doi.org/10.1021/acsmaterialslett.9b00120
38. L.H. Kim, K. Kim, S. Park, Y.J. Jeong, H. Kim et al., Al_2O_3/TiO_2 nanolaminate thin film encapsulation for organic thin film transistors via plasma-enhanced atomic layer deposition. ACS Appl. Mater. Interfaces **6**(9), 6731–6738 (2014). https://doi.org/10.1021/am500458d
39. J. Meyer, H. Schmidt, W. Kowalsky, T. Riedl, A. Kahn, The origin of low water vapor transmission rates through Al_2O_3/ZrO_2 nanolaminate gas-diffusion barriers grown by atomic layer deposition. Appl. Phys. Lett. **96**, 243308 (2010). https://doi.org/10.1063/1.3455324
40. J. Yang, X. Yang, Y. Zhang, B. Che, X. Ding et al., Improved gate bias stressing stability of IGZO thin film transistors using high-k compounded ZrO_2/HfO_2 nanolaminate as gate dielectric. Mol. Cryst. Liq. Cryst. **676**, 65–71 (2019). https://doi.org/10.1080/15421406.2019.1595757
41. Z. Liu, Z. Yin, J. Wang, Q. Zheng, Polyelectrolyte dielectrics for flexible low-voltage organic thin-film transistors in highly sensitive pressure sensing. Adv. Funct. Mater. **29**(1), 1806092 (2019). https://doi.org/10.1002/adfm.201806092
42. D.K. Schroder, *Semiconductor Material and Device Characterization*. pp. 489–502 (A JOHN WILEY & SONS, 2005). https://doi.org/10.1002/0471749095
43. J. Zhang, X. Ding, J. Li, H. Zhang, X. Jiang et al., Performance enhancement in InZnO thin-film transistors with compounded ZrO_2–Al_2O_3 nanolaminate as gate insulators. Ceram. Int. **42**, 8115–8119 (2016). https://doi.org/10.1016/j.ceramint.2016.02.014

44. S.P. Chang, D. Shan, Doping nitrogen in InGaZnO thin film transistor with double layer channel structure. J. Nanosci. Nanotechnol. **18**, 2493–2497 (2018). https://doi.org/10.1166/jnn.2018.14344
45. J. Koo, H. Jeon, Characteristics of an Al_2O_3/HfO_2 bilayer deposited by atomic layer deposition for gate dielectric applications. J. Korean Phys. Soc. **46**(4), 945–950 (2005)
46. L. Zhou, Y. Liu, Q. Liu, B. Qi, Y. Chen et al., Effect of single Hf^{4+} ion substitution on microstructure and magnetic properties of hexagonal M-type $Ba(Hf)_xFe_{12-x}O_{19}$ ferrites. J. Mater. Sci. Mater. Electron. **31**, 4106–4112 (2020). https://doi.org/10.1007/s10854-020-02957-z
47. W. Yang, R. Jiang, Bipolar plasticity of the synapse transistors based on IGZO channel with $HfO_xN_y/HfO_2/HfO_xN_y$ sandwich gate dielectrics. Appl. Phys. Lett. (2019). https://doi.org/10.1063/1.5100128
48. P. Xiao, J. Huang, T. Dong, J. Yuan, D. Yan et al., X-ray photoelectron spectroscopy analysis of the effect of photoresist passivation on InGaZnO thin-film transistors. Appl. Surf. Sci. **471**, 403–407 (2019). https://doi.org/10.1016/j.apsusc.2018.11.211
49. Y. Liu, X. Wang, W. Chen, L. Zhao, W. Zhang et al., IGZO/Al_2O_3 based depressed synaptic transistor. Superlat. Microstruct. **128**, 177–180 (2019). https://doi.org/10.1016/j.spmi.2019.01.026
50. Y. Zhang, Y. Lin, G. He, B. Ge, W. Liu, Balanced performance improvement of a-InGaZnO thin-film transistors using ALD-derived Al_2O_3-passivated high-k $HfGdO_x$ dielectrics. ACS Appl. Electron. Mater. **2**(11), 3728–3740 (2020). https://doi.org/10.1021/acsaelm.0c00763
51. E. Lee, T.H. Kim, S.W. Lee, J.H. Kim, J. Kim et al., Improved electrical performance of a sol-gel IGZO transistor with high-k Al_2O_3 gate dielectric achieved by post annealing. Nano Converg. **6**, 24 (2019). https://doi.org/10.1186/s40580-019-0194-1
52. H. Jung, W.H. Kim, B.E. Park, W.J. Woo, I.K. Oh et al., Enhanced light stability of InGaZnO thin-film transistors by atomic-layer-deposited Y_2O_3 with ozone. ACS Appl. Mater. Interfaces **10**(2), 2143–2150 (2018). https://doi.org/10.1021/acsami.7b14260
53. F. Huang, S.Y. Kim, Z. Rao, S.J. Lee, J. Yoon et al., Protein biophotosensitizer-based IGZO photo-thin film transistors for monitoring harmful ultraviolet light. ACS Appl. Bio Mater. **2**(7), 3030–3037 (2019). https://doi.org/10.1021/acsabm.9b00341
54. C. Dong, G. Liu, Y. Zhang, G. Feng, Y. Zhou, Double-stacked gate insulators SiO_x/TaO_x for flexible amorphous InGaZnO thin film transistors. Mat. Sci. Semicon. Proc. **96**, 99–103 (2019). https://doi.org/10.1016/j.mssp.2019.02.030
55. J. He, G. Li, Y. Lv, C. Wang, C. Liu et al., Defect self-compensation for high-mobility bilayer InGaZnO/In_2O_3 thin-film transistor. Adv. Electron. Mater. **5**(6), 1900125 (2019). https://doi.org/10.1002/aelm.201900125

 https://doi.org/10.1007/s40820-022-00929-y